EEG-based visual deviance detection in freely behaving mice

Renate Kat[a], Berry van den Berg[b], Matthijs JL Perenboom[c], Maarten Schenke[d], Arn MJM van den Maagdenberg[c,d], Hilgo Bruining[e], Else A Tolner[c,d*], Martien JH Kas[a *]

[a]Groningen Institute for Evolutionary Life Sciences (GELIFES), University of Groningen, Nijenborgh 7, 9747 AG, Groningen, the Netherlands, r.kat@rug.nl, m.j.h.kas@rug.nl

[b]Faculty of Behavioural and Social Sciences, Cognitive Neuroscience, Department of Experimental Psychology, University of Groningen, Grote Kruisstraat 2/1, 9712 TS, Groningen, the Netherlands, berry.van.den.berg@rug.nl

[c]Department of Neurology, Leiden University Medical Center, Albinusdreef 2, 2300 RC, Leiden, the Netherlands, M.J.L.Perenboom@lumc.nl, A.M.J.M.van_den_Maagdenberg@lumc.nl, E.A.Tolner@lumc.nl

[d]Department of Human Genetics, Leiden University Medical Center, Einthovenweg 20, 2300 RC, Leiden, the Netherlands.

[e]Department of Child and Adolescent Psychiatry, Amsterdam University Medical Center, University of Amsterdam, Postbus 7057, 1007 MB, Amsterdam, the Netherlands, h.bruining@amsterdamumc.nl

*These authors have contributed equally to this work

Corresponding author:

Prof. Dr. MJH Kas; Groningen Institute for Evolutionary Life Sciences (GELIFES), University of Groningen, Nijenborgh 7, 9747 AG Groningen, The Netherlands m.j.h.kas@rug.nl

Abbreviations ERP: event related potential; MMN: mismatch negativity; TFR: time-frequency reponse; V1: primary visual cortex; VEP: visual evoked potential

Abstract

The mouse is widely used as an experimental model to study visual processing. To probe how the visual system detects changes in the environment, functional paradigms in freely behaving mice are strongly needed. We developed and validated the first EEG-based method to investigate visual deviance detection in freely behaving mice. Mice with EEG implants were exposed to a visual deviant detection paradigm that involved changes in light intensity as standard and deviant stimuli. By subtracting the standard from the deviant evoked waveform, deviant detection was evident as bi-phasic negativity (starting around 70 ms) in the difference waveform. Additionally, deviance-associated evoked (beta/gamma) and induced (gamma) oscillatory responses were found. We showed that the results were stimulus-independent by applying a "flip-flop" design and the results showed good repeatability in an independent measurement. Together, we put forward a validated, easy-to-use paradigm to measure visual deviance processing in freely behaving mice.

Keywords

visual processing, mismatch negativity, sensory processing deficits

1. Introduction

The experiments by Hubel and Wiesel on direction selectivity of neurons in the cat visual cortex (Hubel, 1959; Hubel & Wiesel, 1968) have pioneered a growing scientific field on the visual system and its processing abilities. Since then, the mouse is a widely used animal model to investigate visual processing (Baker, 2013). One important reason is that mice are particularly suitable for genetic modification, such as the use of advanced genetically encoded tools for neuroimaging and neuromodulation that allow unravelling of neuronal network dynamics (Warden et al., 2014). Moreover, transgenic mouse models allow to examine the role of specific cell types or neuronal populations (Sohya et al., 2007; Hamm and Yuste, 2016), as well as to study altered visual processing in the context of human psychiatric disorders (Zhang et al., 2017; Hamm et al., 2020; Perenboom et al., 2020). However, visual processing has hardly been studied in awake, freely behaving mice, as typically head-fixation is used to ensure that visual stimuli reach the eye (Montijn et al., 2016; Carrillo-Reid et al., 2019; Fournier et al., 2020). Assessing measures of visual processing in freely moving mice requires a behavioural setup in which animals are constantly exposed to visual stimuli in their environment irrespective of their bodily position.

Detecting changes in the environment is an important function of sensory systems. The brain can shift attention to changes in the environment via either a passive reduction in the response to redundant stimuli, or an active memory-based increased response to unexpected, or deviant, stimuli (Garrido et al., 2009). The representation of deviance detection in the EEG signal has also been called mismatch negativity (MMN; May et al., 1999). Deficits in deviance detection have been associated with various neuropsychiatric disorders, mainly schizophrenia (Näätänen et al., 2014; Tada et al., 2019). In recent years

it has become clear that a homolog of the MMN is also present in the visual modality, the vMMN (Czigler, 2007; Kimura, 2012; Pazo-Alvarez et al., 2003). The vMMN has gained substantially less attention compared to auditory deviance detection and has only twice been studied in rodents (Hamm and Yuste, 2016; Vinken et al., 2017). While these studies were able to assess vMMN, the animals were required to be head-fixated.

Here we set out to develop a novel paradigm to measure deviance-induced differences in visual evoked potentials (VEPs) in freely behaving mice. Based on MMN oddball concepts used in the context of auditory deviance detection (Harms et al., 2016), our vMMN paradigm involves changes in light intensity as standard and deviant stimuli. In order to use the measured EEG waveform difference features for vMMN, the paradigm needs to comply with three principal criteria. First, the paradigm should be able to elicit a *robust deviance response* as measured through the difference between the deviant versus standard VEP responses. Second, the deviance response needs to be *stimulus-independent,* meaning that the same response difference is found when using either of the two stimuli - in our case increases versus decreases in light intensity – as deviant. Third, the VEP deviance effect needs to be repeatable in an independent measurement within the same subject (*repeatability*). After satisfying the three criteria based on VEP waveforms, characteristics of the frequency responses for the paradigm were explored to gain insight in visual deviance-induced oscillatory activity. In addition, the influence of the repeated light stimulation was explored by assessing how the strength of the observed vMMN changed with increasing number of standards preceding a deviant.

2. Materials and Methods

2.1 Mice

88 Male C57BL/6J mice (n=13) were used to implement and validate the newly developed
89 vMMN paradigm. Animals were single-housed in individually ventilated cages for at least
90 one week prior to surgeries and maintained on a 12:12 light-dark cycle with *ad libitum*
91 access to food and water. All experiments were approved by the Animal Experiment
92 Ethics Committee of Leiden University Medical Center and were carried out in accordance
93 with ARRIVE guidelines and EU Directive 2010/63/EU for animal experiments. All efforts
94 were made to minimize discomfort of the experimental animals.

95 *2.2 EEG implantation surgery*

96 Stereotactic EEG electrode implantation surgery was performed in mice at the age of 2
97 months. Under isoflurane anaesthesia (1.5%, in oxygen-enriched air), three silver (Ag)
98 ball-tip electrodes were implanted epidurally above the right prefrontal cortex (bregma
99 +2.6 mm anterior, -1.6 mm lateral) and the right and left primary visual cortex (V1;
100 bregma -3.5 mm posterior, +/- 3.0 mm lateral). The relatively lateral V1 position was
101 chosen since multiple studies indicate a role for the visual extra-striate areas (which are
102 located more laterally on the occipital cortex) in the vMMN (reviewed in: Kimura, 2012;
103 Vinken et al., 2017). Two epidural platinum electrodes were placed above cerebellum to
104 serve as reference and a ground electrode, respectively. Electromyogram (EMG)
105 electrodes were placed on top of the neck muscles to record muscle activity. Light-
106 activated bonding primer and dental cement (Kerr optibond / premise flowable, DiaDent
107 Europe, Almere, the Netherlands) were used to attach electrodes to the skull. Post-
108 operative pain relief was achieved by a subcutaneous injection of Carprofen (5 mg/kg).
109 EEG recordings started after a 14-day recovery period.

110 *2.3 EEG and VEP recordings*

111 Tethered EEG recordings were performed in a Faraday cage in which animals were
112 connected to the recording hardware via a counterbalanced, low-torque custom-build
113 electrical commutator. Signals were three times pre-amplified, band-pass filtered (0.05
114 to 500 Hz), then amplified 1200 times and thereafter digitized (Power 1401, Cambridge
115 Electronic Devices, Cambridge, UK) at a sampling rate of 5000 Hz. For the recording of
116 VEPs, mice were placed inside a computer-controlled custom-built LED-illuminated
117 sphere in which tethered mice were able to move freely (Van Diepen et al., 2013). The
118 sphere (30 cm diameter) was coated with high-reflectance paint that spread light
119 produced by a ring of white monochromatic LEDs at the top of the sphere around an
120 opening for the swivel. A baffle prevented the mice from looking directly into the LEDs.
121 After connecting mice to the setup in the sphere, animals were allowed to habituate for
122 at least 10 min. Mice were tested once in a baseline assessment and twice in an oddball
123 paradigm, all on separate days. The baseline assessment, in which a train of light flashes
124 of increasing intensity was presented to the animals, was performed to determine VEP
125 signal quality. 60 flashes of 1 ms with increasing light intensity between ~0.4 to 1.1
126 $\mu W/cm^2/nm$ were presented at 2 Hz, and 5 flashes of increasing intensity between ~1.4
127 to 2.2 $\mu W/cm^2/nm$ at 0.5 Hz. The paradigm was repeated 50 times with 20 s rest in-
128 between blocks.

129 *2.4 Visual oddball paradigm*

130 To measure vMMN, a light intensity-based oddball paradigm with decreases and
131 increases in light intensity was developed (Fig. 1). To ensure stable levels of light-
132 adaptation before onset of the oddball sequence, the paradigm started with 10 min of
133 constant light of medium intensity (0.15 $\mu W/cm^2/nm$). Subsequently a 7-minute
134 sequence started in which 300-ms pulses of increased (1.7 $\mu W/cm^2/nm$) or decreased

135 light intensity (0.02 μW/cm^2/nm) stimuli were interspersed by a 500-ms inter-stimulus
136 interval of the 0.15 μW/cm^2/nm constant light intensity (Fig. 1). The constant level of
137 light in between the sequence of standard and deviant stimuli was used to prevent
138 occurrence of dark adaptation between stimuli. The intensities of increases and
139 decreases were chosen based on VEP amplitudes in the grand average baseline curve in
140 such a way that the amplitude change from decrease to ISI level was the same as the
141 amplitude change from ISI to increase level. The stimulus duration of 300 ms was based
142 on earlier vMMN studies that used stimulus durations between 80 and 500 ms, in humans
143 (Stagg et al., 2004; Kimura et al., 2010; Sulykos and Czigler, 2014) and rodents (Hamm
144 and Yuste, 2016; Vinken et al., 2017). Deviant stimuli were semi-randomly spread
145 through the sequence, with the constraint of a minimum of two standard presentations
146 before the next deviant. The first stimulation block in the paradigm contained 500 stimuli,
147 437 (87.4%, the standard) of which were intensity increases and 63 (12.6%, the deviant)
148 of which were light intensity decreases. After this block, the paradigm (including the 10
149 minutes constant light at the start) was repeated with a swap of standard and deviant
150 stimulus type. This so called 'flip-flop' paradigm allowed for assessment of differences
151 between standard and deviant stimuli irrespective of stimulus type (Harms et al., 2016),
152 in our case increased *vs* decreased light intensity. The visual oddball paradigm was
153 performed twice for every animal on separate days. Every animal was once tested in the
154 morning (1st half of the light phase) and once in the afternoon (2nd half of the light phase),
155 whereby the order of the morning and afternoon measurement was counterbalanced
156 over the animals.

157 *2.5 Analysis*

No animals had to be excluded on the basis of low signal quality as judged from the baseline assessment of stimulus responses. For two animals, positive-negative inverted signals were evident on one of the visual cortex electrodes (once right V1 and once left V1); these electrodes were excluded from analysis. Next, recordings were manually checked to exclude recording periods with artefacts, as well as periods of sleep, as deviance detection is known to be attenuated or even absent in non-REM sleep (Sculthorpe et al., 2009). For sleep detection, recordings were first screened for the presence of periods where a passive infrared (PIR) motion detector did not pick up non-specific locomotor activity. If periods without locomotor activity were present during stimulus presentation, they were checked for the presence of non-REM sleep, as defined by high amplitude delta (<4 Hz) waves, so called slow waves, in the frontal EEG signal in combination with an absence of activity in the EMG signal. Two recordings which contained periods of sleep were excluded from analysis (both being the first recording of the animal).

2.5.1 VEP waveforms

Data pre-processing was performed in Matlab (Versions 2018a & 2018b, MathWorks, Natick, MA, USA). EEG data were low-pass filtered at 70 Hz with a fourth order Butterworth filter. For evoked potential waveform analysis, VEPs were extracted from the data of each recording electrode from 50 ms before until 300 ms after stimulus onset. Subsequently, VEPs were grouped into deviant and standard stimuli, irrespective of being a light intensity increase or a light intensity decrease. Within those two categories, trails were averaged, and subsequently baseline corrected, using a latency window that ranged from -50 to 0 to ms prior to the change in light intensity. For plotting purposes, all 437 standard trials were averaged. However, to have a balanced numbers of standards and deviants in the statistical comparisons, bootstrapping of 100 random sets

183 of 63 standards was used in the statistical analysis. Difference waves were calculated by
184 subtracting the standard from the deviant VEP. A comparison between the difference
185 waves of the right and left V1 electrode (using cluster-based permutation analysis) did
186 not reveal any time windows of significant differences (data not shown). In subsequent
187 analyses VEPs from the right and left electrode were averaged. Averaging over trials,
188 electrodes and recordings was performed for the data from individual animals before
189 performing any statistical analysis for the data-sets across animals.

190 To test whether vMMN was significantly different from zero cluster-based
191 permutation analysis was used as previously described (Maris and Oostenveld, 2007). In
192 short, dependent *t*-test statistics were obtained for every time point (0.2-ms steps) of the
193 difference waves and were clustered over time along adjacent points that reached above
194 the *t*-value threshold corresponding to an alpha-level of 0.05. The sum of all *t*-values in
195 a cluster was used as the cluster statistic. To assess significance of these clusters, a 'null'
196 distribution was created by performing 1000 random permutations with the individual
197 animal difference waves and zero. Cluster statistics were extracted for every
198 permutation in the same manner as described above. Both the largest positive and the
199 largest negative cluster from each permutation were used to create two distributions.
200 Clusters in the actual data were considered significant when exceeding the 97.5-
201 percentile threshold for cluster size in either the positive or negative distribution. The
202 permutation process was repeated for difference waves computed with each of the 100
203 randomly selected subsets of 63 standards. The largest cluster for each component (the
204 early (30-70 ms), the late (70-150 ms) and effects after vMMN latencies (> 150 ms)) was
205 saved into a p-value distribution of which the median, the maximum, the minimum and
206 the percentage of p-values below alpha ($p < 0.05$) were reported (median [min max],
207 percentage). Medians were reported instead of means, because the p-values were not

208 normally distributed. When no cluster was found, a value of 1 was added to the
209 distribution.

210 Comparable procedures were used to compare VEP features between right and
211 left electrodes, light intensity increases and decreases, and first and second recordings.
212 However, in these cases permutations were performed by randomly exchanging the data
213 between the two conditions in the comparison. As small numbers of clusters were found
214 for the comparison of the first and second recording, for these data all clusters that were
215 found in the bootstrap were pulled together; for the deviants, no bootstrap was used but
216 all 63 deviants were simply compared between the first and second recording.

217 Cluster-based permutation analysis does not have a good level of precision for
218 finding exact on- and off-sets, therefore borders of the time, as well as time-frequency,
219 windows of reported clusters should be interpreted carefully (Sassenhagen and
220 Draschkow, 2019). Latency windows plotted in the VEP figures display the windows as
221 found by the analysis with all standards.

222 *2.5.2 Time-frequency analysis*

223 For analysis of time-frequency responses (TFRs), single trial data (i.e. from a single
224 stimulation; either a standard or deviant) were extracted from the EEG signal from 1 s
225 before to 1.5 s after stimulus onset. The data was low-pass filtered at 150 Hz. Like with
226 the VEP analysis, trials were grouped into standards and deviants irrespective of the
227 stimulus being a light increase or decrease. Using the FieldTrip toolbox for EEG/MEG-
228 analysis (Oostenveld et al., 2011; Donders Institute for Brain, Cognition and Behaviour,
229 Radboud University, the Netherlands), Hanning window convolution was performed with
230 5-ms time windows on single trials. Frequencies were extracted from 4 - 150 Hz with 1-
231 Hz linear steps. The number of cycles increased from 2 to 10 with increasing frequency.

232 Next, power was converted to a log10 scale and an absolute baseline correction was
233 performed using a window from 200 until 100 ms before stimulus onset as the baseline.
234 This window was chosen to avoid including stimulus related activity that would be
235 smeared (in time) due to the width of the Hanning window. The average time-frequency
236 map of standard trials was subtracted from the average time-frequency map of deviant
237 trials. Additionally, to assess non-phase-locked TFRs, per condition the *average* VEP
238 response was subtracted from individual trials in the time domain before performing the
239 same time-frequency analysis as described above (Cohen, 2014; Park et al., 2018). To test
240 for statistical significance of clusters in the TFR difference maps, cluster-based
241 permutation analysis was used as described above for VEP waveform analysis. T-test
242 statistics were in this case obtained for every time-frequency point (5-ms and 1-Hz steps)
243 and clustered over time and frequency. TFR analysis was performed with the full set of
244 standards.

245 *2.5.3 Exploratory analysis of the effect of preceding number of standards*

246 To explore effects of the number of standards since the last deviant, in other words the
247 number of preceding standards, on visual evoked EEG responses (both VEPs and TFRs)
248 including vMMN amplitude, linear mixed effects modelling was performed (Bates et al.,
249 2015a; Kuznetsova et al., 2017). Mixed models have a significant advantage over
250 traditional regression models since they consider the number of individual trials that
251 contribute to a condition, as opposed to calculating the unpooled means per animal, per
252 condition, and losing this type of information (Gelman and Hill, 2007). Here, fewer
253 observations were available for the higher number of trials since the last deviant. Models
254 were estimated and analyzed using the R-package '*lme4*' (Bates et al., 2015b, RStudio,

version 1.2.5042 (R-version 4.0), Boston, MA, USA; lme4 package version 1.1-27; Bates et al., 2015b) and '*lmerTest*' (Kuznetsova et al., 2017).

The amplitude of the VEP waveforms and power of the TFRs were inspected as a function of the number of trials since the last deviant, for both standards and deviants, and light increases and decreases. The VEP waveform mean amplitudes were extracted from each individual trial in the latency windows that were found to be significant clusters in the evoked potential analysis, resulting in two separate models for an early (40 to 60 ms) and a late (70 to 150 ms) latency window. Similarly, the mean frequency power from each of the TFR clusters (across frequencies and time) that were found to be significant was also extracted. For each measurement type (mV or power) and interval, a linear mixed model was constructed with the following formula:

$$\begin{aligned} \mathrm{mV_n} \mid \text{cluster power}_\mathrm{n} \\ &= \beta_{0.j[n]} + \beta_1 \#\mathrm{trials}_{j[n]} + \beta_2 \mathrm{oddball}_{j[n]} + \beta_3 \mathrm{stimulus}_{j[n]} \\ &+ \beta_4 \#\mathrm{trials.oddball}_\mathrm{n} + \beta_5 \mathrm{oddball.stimulus}_\mathrm{n} + \beta_6 \#\mathrm{trials.stimulus} \\ &+ \beta_7 \#\mathrm{trials.oddball.stimulus} + \epsilon_\mathrm{n} \end{aligned}$$

In this formula, for each trial n, the VEP and TFR amplitudes were described by an intercept β_0, a β_1 which indicates the number of trials since last deviant (1-30), a β_2 which relates to whether the trial was a standard or a deviant and β_3 which indicates whether the trial was a light increase or decrease. Finally, β_4 – β_7 indicates the interactions between number of trials since the last deviant, whether a deviant or standard was presented, and whether the stimulus was a light increase or decrease and ϵ_n is the residual error term. The subscript $_{j[n]}$ would indicate whether the model included a random effect by animal. To establish the random-effects structure of the model we used a procedure in which we started with a full model (containing random slopes per animal

279 for all corresponding fixed effects; including the interaction terms) and subsequently
280 reduced model complexity by stepwise removing random factors (starting with the
281 higher-order interaction terms) until the model did not improve (AIC selection criteria;
282 (Bates et al., 2015a). This stepwise procedure has been shown to result in a 'hybrid'
283 model that avoids overfitting the data while containing relevant random effects (Luke,
284 2017; Matuschek et al., 2017). As a result, the random effect per subject for the
285 interaction between number of trials since last deviant and whether the trial was a
286 deviant or standard was excluded. T-statistics were used to assess statistical significance
287 of model parameters using the Satterthwaite estimation of degrees of freedom as
288 implemented in the R-package '*lmerTest*' (Kuznetsova et al., 2017).

289 *2.5.4 Locomotor activity*

290 Locomotor activity of the mice during the vMMN paradigm was assessed by analyzing
291 the intervals between movement events, recorded by a PIR movement sensor. Detected
292 movement events were divided into baseline (10 minutes before stimulation and the 10-
293 minute inter-block interval) and stimulation events. Events within stimulation blocks
294 where further subdivided into events during the light increase standard block and the
295 light decrease standard block. For all recordings included in the main analysis, mean,
296 maximum and minimum interval were calculated per animals, combined over the first
297 and (when applicable) second recording.

298 Differences in locomotor activity intervals between baseline and stimulation
299 phases, as well as between standard increase and standard decrease blocks were tested
300 with Wilcoxon ranked sum tests, as the data did not pass a one-sample Kolmogorov-
301 Smirnov test for normality. A Benjamini-Hochberg false discovery rate correction for
302 multiple comparisons was applied to the *p*-values for testing the mean, minimum and

maximum values.

VEP figures were constructed in GraphPad Prism (Version 8, GraphPad Software, San Diego, CA, USA). Figures of the TFR were constructed in Matlab (Version 2018a,b). Figures of the mixed linear modelling data were constructed in RStudio. Data in text are presented as mean ± standard deviation. The type of variance presented in figures is specified in the figure legends. For all analyses $p < 0.05$ was considered significant. All data and analysis code (R and Matlab) is available on the OSF data repository (www.osf.io/6bhwf/).

3. Results

3.1 Visual mismatch negativity can be assessed in freely behaving mice

For the development of the vMMN paradigm for freely behaving mice, we designed an oddball paradigm with sequences of 300-ms white light pulses of increased (1.7 $\mu W/cm^2/nm$) or decreased (0.2 $\mu W/cm^2/nm$) light intensity, interspersed by a 500-ms interstimulus interval at constant light of intermediate intensity (0.15 $\mu W/cm^2/nm$, Fig. 1). Deviant stimuli (63 of 500 stimuli, 12.6%) were semi-randomly spread throughout the sequence with the constraint of a minimum of two standard presentations before the next deviant. In the paradigm both increases and decreases in light intensity were presented once as standard and once as deviant ('flip-flop' paradigm; Harms et al., 2016, Fig. 1). The paradigm was presented twice, on separate days. For the first analysis, VEP responses were averaged for, respectively, all standard and deviant stimuli, regardless of being a response to a light increase or light decrease. VEPs recorded from the right and left primary visual cortex (V1), and the first and the second measurement were combined.

Visual inspection of the averaged VEPs revealed a clear distinction between standard and deviant waveforms (Fig. 2A). Both for deviant and standard stimuli, VEPs showed an initial N1 negativity around 30 ms after stimulus onset, followed by a broad

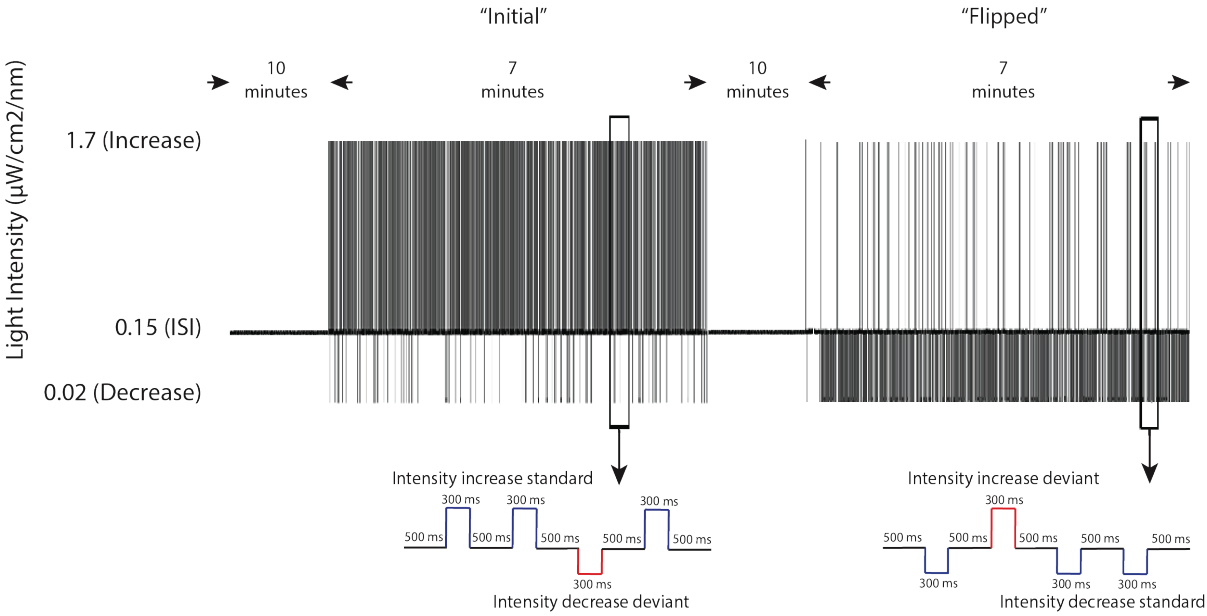

Figure 1 Graphical representation of the light-intensity oddball paradigm used for visual mismatch negativity in freely behaving mice. Mice were presented with an oddball paradigm with increases (1.7 µW/cm²/mm) and decreases (0.02 µW/cm²/mm) in light intensity as stimuli, with intermittent intermediate intensity levels (0.15 µW/cm²/mm). The paradigm was presented as a 'flip-flop' in which the "initial" presentation with intensity increase standards and intensity decrease deviants (left), was followed by a "flipped" presentation with intensity decrease standards and intensity increase deviants (right). Initial and flipped stimulation blocks lasted ~ 7 min each. Before the initial stimulation block and in between the initial and flipped stimulation blocks, 10 min of constant intermediate light (0.15 µW/cm²/nm) was presented. For the analysis, standards of increased intensity were compared to deviants of increased intensity, and standards of decreased intensity are compared to deviants of decreased intensity.

positivity between ~50 and ~150 ms. Compared to the response to standard stimuli, the deviant N1 deflection was slightly broadened, while the later broad positivity was of lower amplitude than observed for the standard response. Consequently, the difference wave, computed by subtracting the standard from the deviant response, consisted of a bi-phasic negative component, between ~35 and ~150 ms, with a maximum peak amplitude

346 of -0.048 ± 0.027 mV (Fig. 2B). Cluster-based permutation analysis revealed two
347 deviance-associated components. The early negative component in the difference wave,
348 ~35-60 ms after stimulus onset, was not significantly different from zero (median p =
349 0.069, [min: 0.024 max: 0.116], percentage < 0.05: 13%), whereas the late negative
350 component, ~70-150 ms after stimulus onset, was (p = 0.010, [<0.001 0.052], 99%). Our
351 visual oddball paradigm thus meets the first criterion of *yielding a robust deviance*
352 *response*, as a significant difference in the response to deviant compared to standard light
353 stimuli could be assessed from VEPs recorded from V1 in freely behaving mice. Compared
354 to the V1 EEG recordings, the oddball paradigm elicited no apparent VEP responses at the
355 prefrontal electrode, nor a distinguishable difference wave (data not shown), indicating
356 specificity of the test paradigm to the visual system.

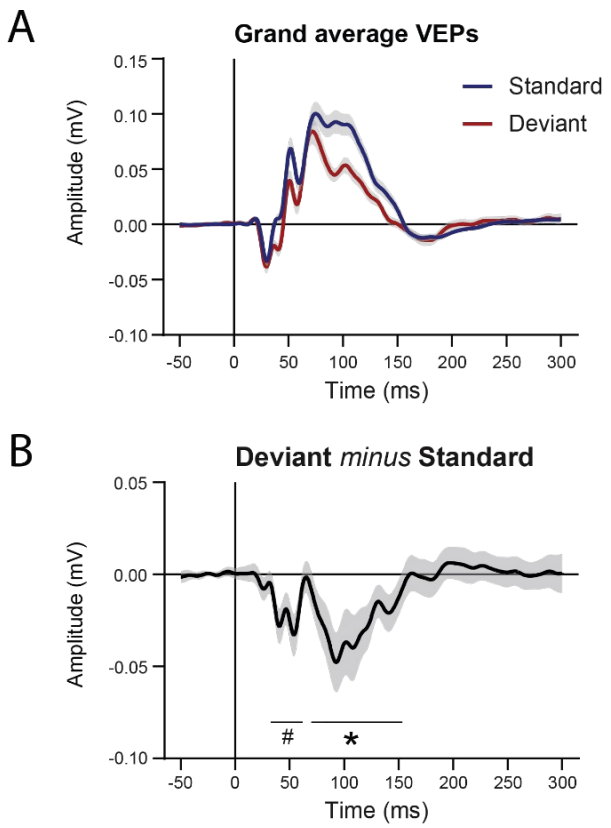

357 **Figure 2 Visual mismatch negativity in the**
358 **visual evoked potential responses to an**
359 **intensity oddball paradigm in freely behaving**
360 **mice. (A)** Grand average VEP waveforms in
361 response to standard and deviant stimuli.
362 Responses were averaged for, respectively, all
363 standard or all deviant stimuli, independent of the
364 standard or deviant representing a stimulus of
365 increased or decreased light intensity. Responses
366 of the right and left V1, as well as the first and
367 second recording were combined. Data are
368 presented as mean ± standard error of the mean
369 (SEM). **(B)** Deviant minus standard difference
370 wave for the combined 'intensity increase' and
371 'intensity decrease' deviants and standards. Data are presented as mean ± 95% confidence interval. Gray
372 shading represents the variance between animals. n = 13, *p<0.01, #p<0.1.

373 *3.2 Visual mismatch negativity in the late VEP component is stimulus-independent*

374 To meet the mismatch negativity criterion of stimulus-independency, the difference
375 between VEP responses to standard and deviant stimuli of intensity increases and
376 intensity decreases should contain similar components. Visual inspection of the standard
377 and deviant VEP waveforms (averaged over the responses from V1 left and right, and the
378 two different recording days) revealed different features in the context of intensity
379 increase or decrease stimuli, in particular with respect to the early latencies. Specifically,
380 the VEP in response to an intensity increase, for both standard and deviant stimuli,
381 contained additional early latency components between 20 and 60 ms that were not
382 evident in the VEP in response to an intensity decrease (Fig. 3A).

383 While the early components of standard and deviant VEP waveforms for light
384 increases and decreases differed, when subtracting the standard from the deviant
385 response for stimuli of the same light change (i.e. increase or decrease), the deviant-
386 minus-standard difference waves appeared remarkably similar for both light intensity
387 changes with respect to the late component around 100 ms (Fig. 3B). However, the late
388 component of the difference wave, at a latency range of ~70-150 ms, was significantly
389 different from zero for the intensity increase (p = 0.006, [<0.001 0.036], 100%), but did
390 not reach significant for the intensity decrease responses (p = 0.065, [<0.001 0.242],
391 42%). The early component of the difference wave was only evident in the difference
392 wave of an intensity increase (p = 0.030, [0.004 0.072], 89%); decrease: p = 0.603, [0.106
393 1.00], 0%). For the difference wave of the intensity decrease responses, the shape of the
394 early component was visible but did not differ in amplitude from zero (p = 0.603, [0.106
395 1.00], 0%). After 150 ms, the difference waves from the intensity increase and decrease
396 responses showed slow shifts in opposite direction which was most evident beyond the
397 ~200 ms latency range of the original VEPs (intensity increase: p = 0.149, [0.010 1.00],

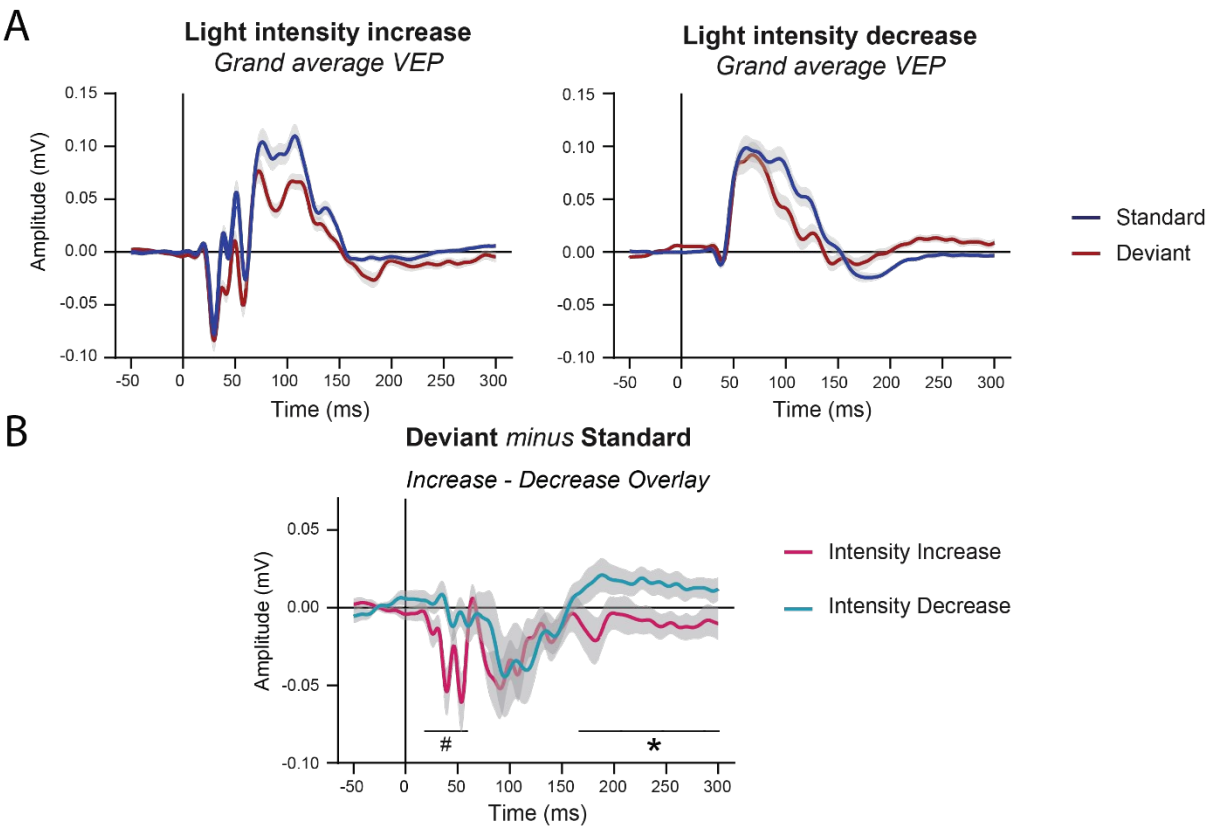

Figure 3 Visual mismatch negativity in the visual evoked potential responses to light pulses of increased or decreased intensity. (A) The VEP waveforms for, respectively, 'intensity increase' (left) and 'intensity decrease' (right) deviants and standards. Data are presented as mean ± standard error of the mean (SEM). (**B**) Overlay of the intensity increase and intensity decrease difference waves. The early negative wave component between 20-60 ms is present only in the difference wave for intensity increase deviants and standards, the late negative wave component around 100 ms is present in both difference waves. A trend level difference between the two difference waves is observed for the early latencies between 20-60 ms. For latencies between 170-300 ms, the waveforms of the intensity increase and decrease difference waves are significantly different. Data are presented as mean ± 95% confidence intervals. Responses were averaged for right and left V1, as well as the first and second recording. Error bars represent the variance between animals. n = 13, *p<0.01, #p<0.1.

25%; intensity decrease: $p = 0.016$, [<0.001 1.00], 65%). When comparing the features of the light increase and the light decrease difference waves directly, the early component was found to differ significantly on a $p < 0.1$ level (~20-60 ms, $p = 0.09$, [0.012 1.00], 16% smaller than 0.05, 57% smaller than 0.1). Despite the fact that the late component was

414 significantly different from zero for the intensity increase but not the intensity decrease,
415 no differences between the intensity increase and decrease were found for the late
416 component (p = 0.368 [0.12 1.00], 0%). In addition, outside the identified window of
417 deviance detection (~30-150 ms), a significant difference between the intensity increase
418 and decrease difference waves was found for the additional late component between
419 ~170-300 ms (p = 0.008 [<0.001 1.00], 83%). In conclusion, although both the early and
420 the late latency component were more pronounced in light intensity increase difference
421 waves, the late negative component at ~100 ms could not be statistically differentiated
422 between the responses to light intensity increases and decreases. With the use of this
423 component of the deviant-minus-standard difference waves, our vMMN paradigm thus
424 satisfies our second criterion of *stimulus independency*.

425 The comparison of the intensity increase and decrease responses also revealed,
426 perhaps not surprisingly, that the 'off-response' to an intensity increase – in essence
427 being an intensity decrease – showed a VEP similarly shaped as the 'on-response' of the
428 intensity decrease and vice versa (Supplementary Fig. 1). Increases and decreases in light
429 intensity thus seemed to be processed as *shifts* in light intensity rather than as flashes of
430 *different* intensities. The on- and off-responses to a light increase showed slightly higher
431 amplitudes compared to the on- and off-responses to a light decrease. The chosen
432 magnitude of the intensity shifts, which was larger for increases than decreases (i.e. a
433 shift from 0.15 to 1.7 compared to 0.15 to 0.02 μW/cm^2/mm), was selected based on tests
434 with a 1-ms flash VEP paradigm that showed an equal amplitude difference for both
435 increase and decrease intensities compared to the VEP amplitude response to the ISI
436 intensity. However, in the deviant paradigm the larger intensity shifts still evoked a
437 slightly higher amplitude response. As the latencies of all identified deviance detection
438 components fall within the 300-ms duration of the light stimuli, these off-responses do

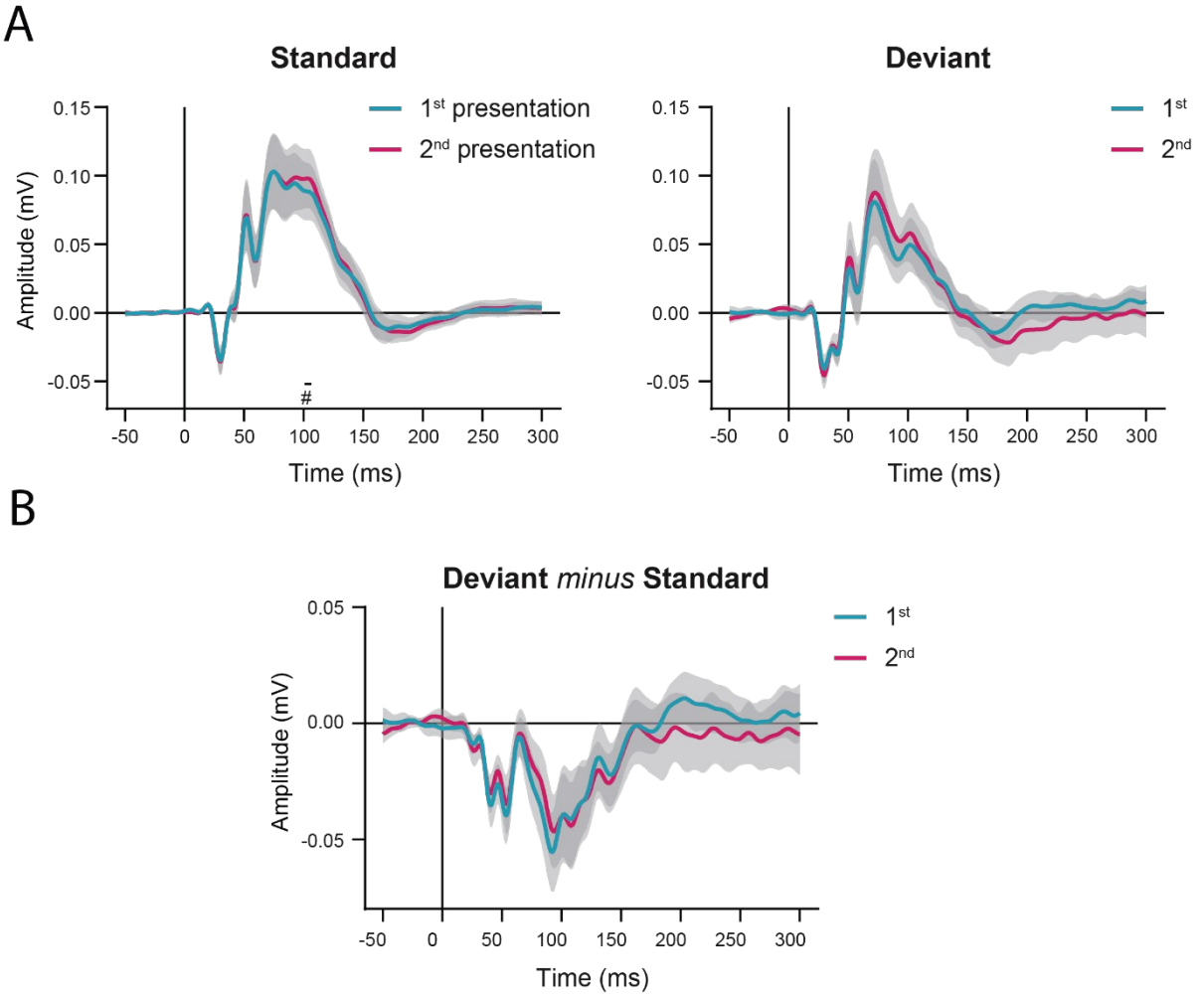

Figure 4. Comparison of the visual evoked potential responses from the 2 independent measurements. The same light intensity oddball paradigm was presented to all mice twice, on separate days (i.e. 1st and 2nd presentation). **(A)** VEPs in response to standard and deviant stimuli, averaged for, respectively, the 1st and the 2nd presentation. **(B)** Overlay of the deviant minus standard difference waves. n = 11, data are presented as mean ± 95% confidence interval. Gray shading represent the variance between animals. Cluster-based permutation analysis did not reveal any significant differences between the 1st and the 2nd presentation.

not affect our deviance detection.

3.3 Visual mismatch negativity shows repeatability in an independent measurement

Our third criterion for a vMMN paradigm concerns repeatability of the outcome in independent measurements. To assess this, each animal was subjected to the visual

oddball paradigm twice on two separate days. Using cluster-based permutation analysis, no differences between the first and second recording were observed for either the standard VEPs, deviant VEPs or difference waves for the combined responses to intensity increases and decreases (Fig. 4). For both the standard VEP and the difference wave, only four percent of the clusters found after bootstrapping with random subsets of standards was smaller than 0.05, of which all but one had a latency of more than 150 ms (difference wave: p = 0.498 [0.010 0.988], 4.1%; standard: p = 0.490 [0.006 0.938], 4.0%). For the deviant, two clusters were found (p = 0.814/0.608). These outcomes indicate that our visual oddball paradigm has a good *test-retest reliability* and therefore also meets the third criterion.

3.4 Mice show intrinsic drive for locomotor activity during visual stimulation

An advantage of using a freely behaving set-up is the opportunity to assess spontaneous behaviour during the EEG recordings. Mice in our vMMN paradigm turned out to show relatively constant high locomotor activity levels during recordings. An exception to this were two mice which were asleep during part of the first recording session, the recordings of which were excluded from further analysis. For the remaining recordings of all mice, periods of inactivity were rare and the overall average interval between two locomotor activity events (as registered by PIR movement sensors in the setup) was only 0.83 ± 0.02 seconds. The occurrence of VEPs during periods inactivity was too infrequent to allow correlating VEP features with expression of locomotor activity. While no differences were found for the mean and minimum locomotor activity interval between baseline (i.e. sum of the 10 minutes before the first stimulation block and the 10 minute-interval between both stimulation blocks) and stimulation blocks of the paradigm (mean: Z = 1.33, p = 0.273; minimum: Z = -0.67, p = 0.505), the maximum locomotor activity

interval was lower during the blocks with visual stimulation (Z = 3.08, p = 0.006; Figure 5a). When comparing the stimulation block in which intensity increases served as standards with the block in which intensity decreases served as standards, no differences in any of these locomotor activity measures were found (mean: Z = -0.46, p = 0.644; minimum: Z = -1.08, p = 0.422; maximum: Z = -1.64, p = 0.302; Figure 5b). Thus, during the EEG assessments in the light sphere, mice showed a high drive for locomotor activity which increased slightly during the stimulation periods.

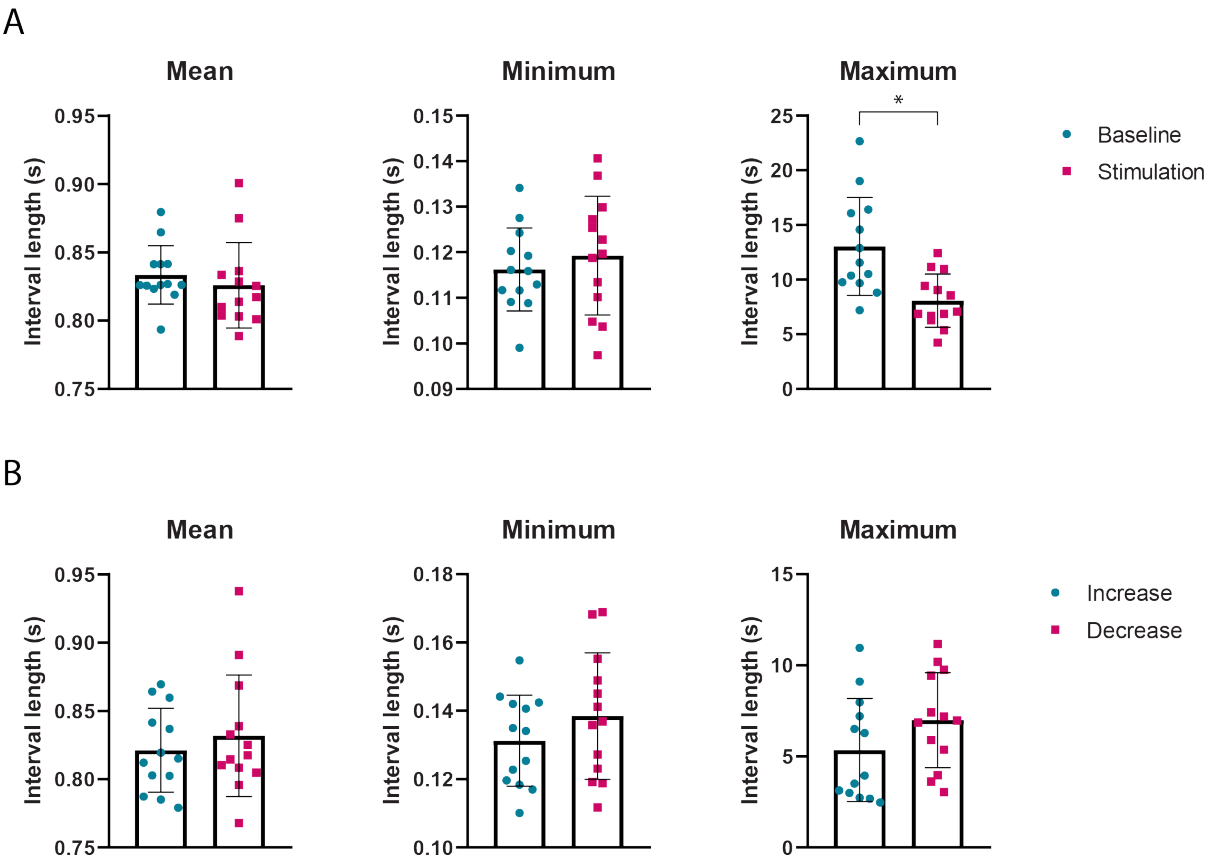

Figure 5. Locomotor activity during EEG assessments in the freely behaving visual stimulation set-up. PIR-movement sensors inside the light spheres registered time-stamped events whenever movement was detected. The intervals between consecutive movement events were calculated for all animals. **(A)** Mean, minimum and maximum movement interval lengths during baseline (blue circles) and stimulation (pink squares) periods. **(B)** Mean, minimum and maximum movement interval lengths during the blocks with respectively intensity increases (blue circles) or decreases (red squares) as standard. N = 13, data are presented as mean ± standard deviation with individual data points. * $p < 0.05$

3.5 Visual deviance detection is also evident from the light-triggered time-frequency response

In addition to examining VEP waveform features from the deviant-standard difference waves, we analysed the EEG TFR. Human studies showed that vMMN has oscillatory components that are not phase-locked to the stimulus and would therefore cancel out when averaging over trials, which is part of classical event-related potential (ERP) analysis (Stothart and Kazanina, 2013). TFRs are time-locked, but in contrast to ERP waveforms, not necessarily phase-locked to the stimulus and can therefore give a more complete picture of stimulus-associated activity. Visual inspection of the frequency spectra in response to standards and deviants revealed activity in several frequency ranges. The EEG response to standard stimuli – combined for intensity increases and decreases – showed an apparent increased power for the beta-lower gamma (~20-40 Hz, labelled with '1' in Fig. 6A) and the gamma range (~50-100 Hz, labelled with '2' in Fig. 6A) at a latency between ~20 and ~70 ms after stimulus onset. In addition, a broad increase in power was seen for the theta range (~4-9 Hz, labelled with '3' in Fig. 6A), evident from stimulus onset to a latency of ~200 ms. While the TFR to deviant stimuli showed an overall comparable pattern (Fig. 6A), comparison between deviant and standard TRFs in a deviant minus standard heatmap revealed multiple clusters with significantly different frequency components (Fig. 6A). Most evident was a cluster between ~20-120 ms, indicating increased EEG power in the range from ~10-70 Hz in response to deviants (p = 0.022, labelled with 'A' in Fig. 6A). This cluster seemed to be the result of a combination of an altered shape of the beta/gamma response (labelled with '1') to the deviant compared to the standard stimuli, as well as an additional deviant response in the alpha/beta band (~10-20 Hz, labelled with '4' in Fig. 6A) which was not

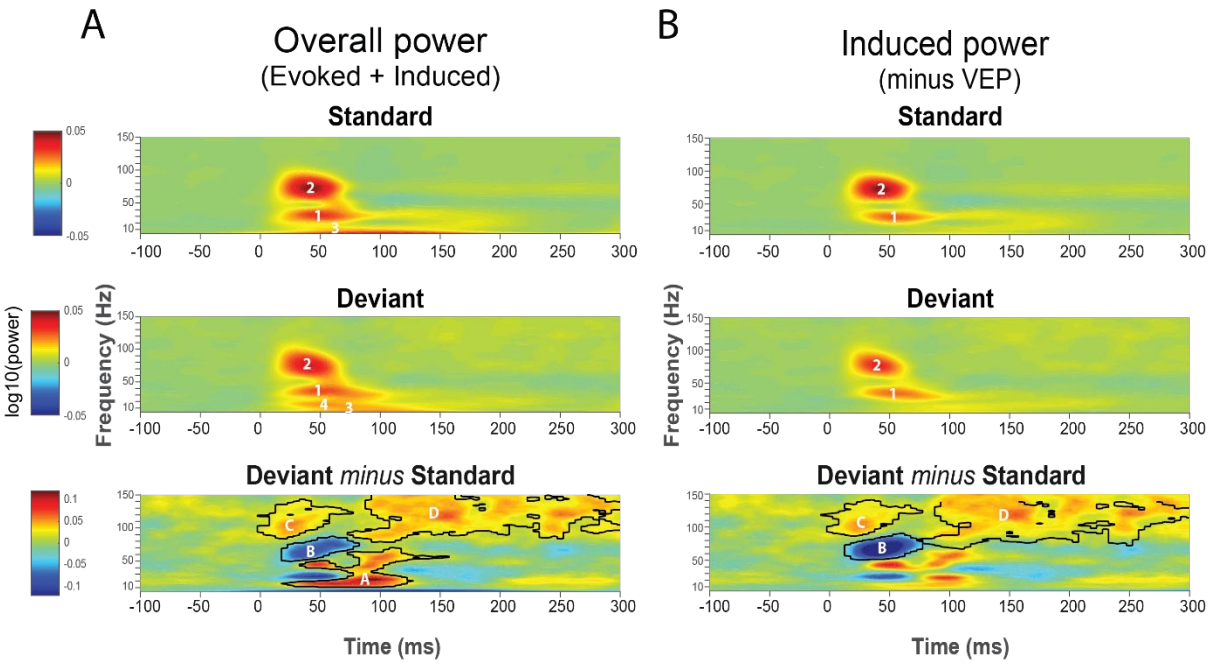

Figure 6. Visual mismatch negativity in the time-frequency response. Panels show clusters of the power of both overall oscillatory activity **(A)**, as well as induced oscillatory activity **(B)** in the vMMN paradigm. To isolate induced oscillatory activity, the averaged waveform was subtracted from each individual trial before running a time-frequency analysis. From top to bottom panel time-frequency responses to standard stimuli, deviant stimuli, and a deviant minus standard difference plot are shown. TFRs were obtained by performing Hanning-window convolution 4-150 Hz with 5 ms time steps. Absolute baseline-correction was performed using -0.2 - -0.1 ms as the baseline. TFRs to light increases and decreases, the right and left V1 as well as and second recording were averaged. Y-axis lower cut-off is 4 Hz. In the difference plot, significant ($p<0.05$) time-frequency clusters are outlined. n=13.

evident in the response to the standard. The gamma response (~50-100 Hz) contained less power in response to deviant compared to standard stimuli (p = 0.048, labelled with 'B' in Fig. 6A). Lastly, increased EEG power in the high gamma range (~80-150 Hz) was seen in response to the deviant compared to the standard, both shortly following stimulus onset between ~0-60 ms (p = 0.036, labelled with 'C' in Fig. 6A) and in a later window between ~90 and ~300 ms (p = 0.002, labelled with 'D' in Fig. 6A).

Oscillatory activity can be divided into evoked power, which is the direct frequency representation of the VEP waveform response, and induced power, which is

532 the oscillatory activity that is non-phase-locked to the stimulus and thus not found in the
533 VEP waveforms (Jones, 2016). To asses which oscillatory clusters in our analysis
534 represented induced power, the time-frequency analysis was also ran after subtracting
535 the average VEP waveform from every single trial per condition (Park et al., 2018).
536 Clusters 3 and 4 in the TFR and cluster A in the difference plot were not present when
537 using this analysis (Fig. 6B) and thus represent evoked power. On the other hand, clusters
538 1 and 2 in the TFR and clusters B, C and D in the difference plot were still present after
539 running time-frequency analysis on mean-subtracted data and represent the power of
540 induced oscillatory activity. With our visual oddball paradigm in freely behaving mice,
541 deviance detection was thus not only reflected in the VEP waveforms, but also in evoked
542 as well as induced power in the EEG time-frequency responses.

543 *3.6 Higher numbers of standards preceding a deviant strengthen visual mismatch negativity*

544 In light of the ongoing debate about the role of adaptation to the repeatedly presented
545 standards in deviance detection paradigms (Garrido et al., 2009; Grimm et al., 2016), we
546 assessed whether stimulus history influenced our VEP-based vMMN. Using linear Mixed
547 effects models (Bates et al., 2015b; Gelman and Hill, 2007) we explored whether the
548 vMMN amplitude (VEP- and TFR-based) changed with varying numbers of standards
549 preceding the deviant. In addition, we assessed whether this was potentially also affected
550 by the stimulus types, i.e., an intensity increase or decrease. The mean amplitude and
551 oscillatory power of standard and deviant VEPs and TFRs were extracted from each trial,
552 for both the cluster-based defined early (40-60 ms) and late (70-150 ms) latency
553 windows rounded to the nearest ten, and the identified gamma (B, ~50-100 Hz) and high
554 gamma (C and D, ~80-150 Hz) induced frequency clusters. We subsequently analysed the
555 amplitude or power using a linear mixed model with the factors 'oddball' (standard,

A

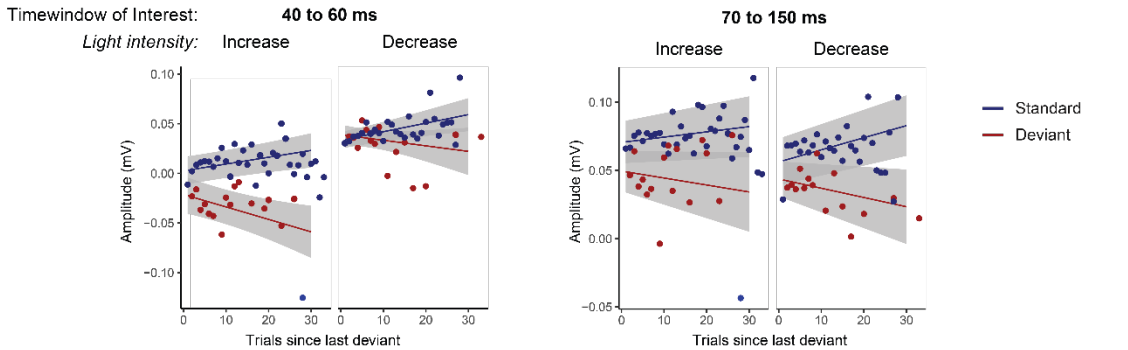

B

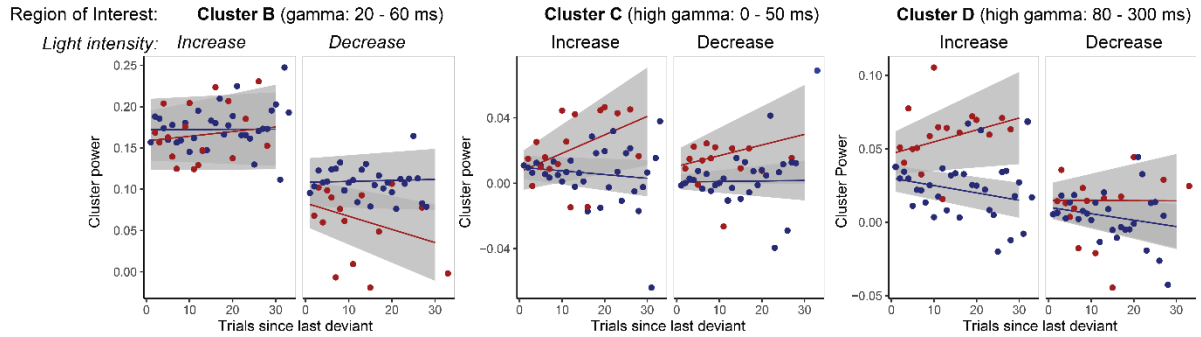

Figure 7. Exploration of effects of stimulus history on VEP- and TFR-based mismatch negativity features. Analyses were performed for the earlier found VEP **(A**, separated for the early and late negativity**)** and TFR **(B)** components. Each of the different graphs depicts the mean amplitude (for VEP features) or power (for TFR features) as a function of the number of preceding standards since the occurrence of the last deviant. For both VEP and TFR features, the vMMN amplitude (for VEP) or power (for TFR) is the difference between the standard and deviant amplitude, which for the early and late VEP component and TFR cluster B was found to increase with an increasing number of preceding standards. Data are presented separately for standard and deviant stimuli, as well as for intensity increases and decreases. n = 13, data are presented as mean ± 95% confidence interval.

deviant), 'stimulus' (light increase, decrease), and 'number of trials since last deviant' (1-30; continuous and linear variable).

Early negativity (40-60 ms): amplitudes of the vMMN (deviant minus standard) in the early latency increased with the number of trials since the last deviant ($1.684*10^{-3}$

570 mV (SE: $0.338*10^{-3}$) per trial). In other words we observed an increase in the early
571 latency vMMN amplitude with longer stretches of standard trials (oddball × # of trials
572 since last deviance: t(25956) = 4.98, $p < 0.001$, Fig. 7A). The amplitude in response to
573 standard VEPs increased with number of trials since last deviant ($0.775*10^{-3}$ mV (SE:
574 $0.176*10^{-3}$) per trial; t(14.9) = 4.41, $p < 0.001$) and the amplitude in response to deviant
575 VEPs decreased ($-0.909*10^{-3}$ mV (SE: $0.342*10^{-3}$) per trial; t(211.9) = -2.66; $p = 0.008$).
576 Furthermore, we confirmed our earlier observation that the amplitudes in the early
577 latency window, irrespective of stimulus history, were stimulus specific (oddball ×
578 stimulus type: t(25956) = 4.72, $p < 0.001$; light increase: deviant minus standard: -0.0368
579 mV, SE = $4.35*10^{-3}$; t(20.6) = 8.46, $p < 0.001$; light decrease: deviant minus standard: -
580 0.0039 mV, SE = $4.35*10^{-3}$; t(20.7) = 0.898, $p > 0.380$).

581 *Late negativity (70-150 ms):* amplitudes of the vMMN in the late latency window
582 paralleled the observations for the early component with respect to a modulation of the
583 vMMN by stimulus history (oddball × trials since last deviant: (1.232 mV (SE: $0.390*10^{-}$
584 ^{3}); per trial; t(25944) = -3.16, $p = 0.002$). While the amplitude of the late negativity
585 response to standard VEPs increased with decreasing novelty ($6.370*10^{-3}$ mV (SE:
586 $0.180*10^{-3}$) per trial; t(14.9) = 3.53, $p = 0.003$), for the deviant responses, the late
587 negativity amplitude did not show a significant decrease in amplitude ($0.060*10^{-3}$ mV
588 (SE: $0.383*10^{-3}$); t(284.3 = 1.55, $p > 0.122$), contrary to what was observed for the early
589 negativity. In the late latency window no overall effect of stimulus type on deviant
590 processing was observed (oddball × stimulus type: t(25944) = -1.19, $p = 0.235$). To
591 further address the stimulus independency, it was tested whether the effects of stimulus
592 history on the late component differed between the stimulus types (i.e. light increase vs
593 light decrease). Addition of this interaction to the model did not improve the fit of the
594 model (ΔAIC = +5.4; ΔBIC = +28, a smaller AIC indicating improvement of the model

weighting complexity [number of parameters] and explained variance), supporting the claim that the amplitudes in the late component were indeed stimulus non-specific.

Oscillatory clusters: for the TFR-based analysis only the early high gamma cluster (C, 80-150 Hz) showed a significant relationship between stimulus history and deviance detection (C: oddball × trials since last deviant $t(25977) = 2.05$, $p = 0.041$; D: oddball × trials since last deviant: $t(25959) = 1.72$, $p = 0.086$, Fig. 7B). However, the large variation and p-values close to the significance threshold suggest that these analyses were underpowered and therefore should be interpreted carefully.

4. Discussion

Mismatch negativity is an important function of the brain to identify environmental changes that may require subsequent appropriate behavioural and/or physiological responses. The goal of this study was to develop and validate a method for assessing vMMN in freely behaving mice. The developed paradigm met all three pre-defined criteria: *a robust deviance response, stimulus-independence,* and *repeatability. First*, the light intensity-based oddball paradigm evoked a bi-phasic negativity in the VEP difference wave, of which the late 70-150 ms component was significantly different from zero, indicating that the paradigm was able to assess the ability of mice to differentiate between standard and deviant flashing light stimuli. *Second*, vMMN in this late component was found to be independent of the type of stimulus (i.e., light increase or decrease) that was used a deviant. *Third*, the paradigm showed good repeatability in a second recording performed on a separate day.

The vMMN presented with our paradigm matches well with previously reported vMMN features from both human and rodent EEG. The only other EEG-based vMMN study in mice, in which a pattern-based oddball paradigm was used in head-fixed animals, also showed bi-phasic responses (Hamm and Yuste, 2016). They identified the differences in response to standard and deviant stimuli in early latencies to reflect stimulus-specific adaptation, while differences in later latencies reflected deviance detection activity. Also human visual ERP studies indicated that early components of sensory processing represented adaptation effects, while later components were specifically associated with violations of expectation (Czigler et al., 2006; File et al., 2017). The onset and timing of the early and late phases differed for each of the studies, as well as the present study, both between and within species. Besides differences in neuronal pathways between species, deviance detection latencies may also be influenced by the stimulus complexity (Kojouharova et al., 2019). For example, Hamm and Yuste (2016), which used visual pattern stimuli instead of the light flashes used in our study, found longer latencies (between ~ 40 and 240 ms) in their mouse visual deviance detection features compared to the latencies observed in our paradigm. In our freely-moving deviance detection paradigm, we could not assess the contribution of stimulus-specific adaptation, as the 'many standards control paradigm' (Czigler et al., 2006; Hamm and Yuste, 2016; Harms et al., 2016; File et al., 2017) was not used. We were however able to show that the early component was sensitive to stimulus properties (i.e. a significant deviance detection effect was only present for light intensity increases), while the late component was stimulus-type-independent. Additionally, the effect of stimulus history on vMMN amplitude was larger for the early compared to the late component. The finding of larger effects of stimulus history and stimulus-specificity on the early component are in line with the previously reported stimulus-specific adaptation in the early latencies and

642 deviance detection in the later latencies (Czigler et al., 2006; File et al., 2017; Hamm and
643 Yuste, 2016). We therefore speculate that also in our paradigm the early component is
644 primarily driven by stimulus-specific adaptation, while the late component represents
645 active deviance detection. Taken together, our vMMN matches well with that observed in
646 humans as well as in mice. Our data show that head fixation is not required for measuring
647 vMMN in mice, and that the implemented paradigm and observed responses in mice have
648 translational value.

649 Performing sensory processing assessments in freely behaving animals does not
650 only reduce stress effects but also increases behavioural relevance and can potentially
651 provide more insight via inclusion of behavioural data. In the current study, locomotor
652 activity levels of the experimental animals were recorded during the VEP assessments.
653 This revealed that during the experiments in the light sphere, mice show a high intrinsic
654 drive for locomotor activity as they showed high levels of activity during the entire
655 recording session. Locomotor activity levels were slightly increased during the periods
656 in which standard or deviant light flashes were presented, as in these periods the
657 maximum locomotor activity intervals were lowered. Since inactive periods were rare,
658 we could not perform separate analysis of VEPs and related deviant features during
659 active and inactive periods. It is important to note that vigilance state scoring for
660 exclusion of periods with sleep was only performed on the stimulus presentation
661 windows, which could have slightly biased our analysis. It has previously been shown
662 that locomotor activity affects EEG in rodents (Hansen et al., 2019), however it is unlikely
663 that locomotion contributed to the difference we found between the shape of increase
664 and decrease VEPs since the amount of locomotor activity was equal between both light
665 increase and decrease stimulation blocks. Increasing habituation periods in the set-up, or
666 increasing the duration of the vMMN paradigm might allow for a comparison between

667 VEP and deviant features during active and inactive periods in future experiments. While
668 assessing visual evoked brain activity during full-field visual stimulation is in our view a
669 logic first step, a future goal would be to develop more naturalistic set-ups where
670 ecologically relevant visual input is presented in such a way that the perception of such
671 input is dependent on the animal's behaviour.

672 VEPs in response to intensity increases and decreases showed different features
673 in particular for the early components. Rather than being processed as flashes of different
674 intensities, based on the off-responses, the used stimuli seemed to be processed as shifts
675 in light intensity. While the processing of different levels of light intensity (Lopez et al.,
676 2002; Perenboom et al., 2020) and its dependence on light-adaptation (Suzuki et al.,
677 1972) have been studied in mice and cats, little is known on how shifts in light intensity
678 are processed. One early study described the presence of off-responses, which were,
679 contrary to what we observed, of similar shape as on-responses, when light flashes (i.e.
680 increases in light intensity) lasted more than 100 ms (Crescitelli and Gardner, 1961).

681 Exploratory analysis of the effect of stimulus history showed that an increased
682 number of trials since the last deviant, in other words a longer stretch of preceding
683 standard presentations, increased the amplitude of the vMMN. This was the result of an
684 increased amplitude of standard VEP responses and a decreased amplitude of deviant
685 VEP responses with a higher number of preceding standards. These changes seem to
686 suggest that our VEP-based deviance detection paradigm was sensitive to short-term
687 novelty of the deviant; as it showed larger responses when the previous deviant was
688 presented a longer time ago. The observed positive relationship between vMMN
689 amplitude and number of preceding standards could be a result of stimulus-specific
690 adaptation of the standard, in our paradigm leading to increased amplitudes after more

691 repetitions. It was slightly unexpected that adaptation to the standard after stimulus
692 repetition presented as an increase in amplitude, instead of depression of the responses.
693 This could be interpreted as a sensitization or tuning of the visual cortices to a specific
694 stimulus as shown by others (Clapp et al., 2006; Solomon and Kohn, 2014). While
695 depression-dominated adaptation to visual stimuli has been shown in anaesthetized
696 animals (Keller and Martin, 2015; Sanchez-Vives et al., 2000), a recent study showed that
697 in awake mice certain types of cortical interneurons show depression-dominated while
698 others show sensitization-dominated adaptation, the strength of which changed with
699 locomotion. As a result, the pyramidal responses could be sensitized as well as depressed
700 (Heintz et al., 2020). Alternatively, larger deviance detection after more preceding
701 standards could result from the brain's response to the violation of a stronger memory-
702 based expectation of the standard (Garrido et al., 2009). Although counterintuitive,
703 violation-alerting activity in our data would actually be represented by the observed
704 reduction in deviant amplitude, resulting in an increased difference with a standard.
705 Further studies are needed to determine which of these two processes primarily drives
706 the deviance detection features in our paradigm. Larger differences in responses to
707 standard and deviant visual pattern stimuli with more preceding standards have
708 previously also been shown in rats, although this difference was dominantly driven by
709 alterations in the responses to the deviant stimuli, without a change in responses to the
710 standard (Vinken et al., 2017). Also in human auditory MMN paradigms the amplitude of
711 the MMN increases when the overall probability of deviants is decreased from 30% to
712 10% or from 13% to 1.5% (Sato et al., 2000; Sabri and Campbell, 2001), as well as with a
713 higher number of standards preceding a deviant within a paradigm with a stable overall
714 deviant probability of 20% (Matuoka et al., 2006). Together, these findings suggest that
715 the effect size of our vMMN paradigm could be further increased by having a higher

716 minimum number of standards between deviants than the two currently used in our
717 experiments.

718 In addition to the VEP waveforms, visual deviance detection was also found to be
719 represented in both evoked and induced oscillatory activity. Human visual and mouse
720 auditory studies have previously shown oscillatory responses related to deviance
721 detection, but the paradigms and corresponding responses showed large variability
722 (Stothart and Kazanina, 2013; Ahnaou et al., 2017; Hesse et al., 2017; Yan et al., 2017).
723 Differences across paradigms and species, as well as the fact that some of these studies
724 use auditory while others use visual stimuli, make a direct comparison of findings from
725 the studies assessing frequency response in deviance detection paradigms difficult.

726 In the TFR the higher gamma clusters between 50-150 Hz represented induced
727 (i.e. non-phase-locked) oscillatory activity. This is in line with the fact that induced power,
728 thought to represent top-down connections, concerns higher frequencies over longer
729 latencies, while evoked power of the visual evoked responses, thought to represent
730 bottom-up connections, concerns lower frequencies over shorter latencies (Chen et al.,
731 2012). The broad increase in high gamma power (80-150 Hz) showed a tendency to be
732 enhanced with more preceding standards, although this effect was not statistically
733 significant Although the role of the various frequency bands in specific functional
734 processes is not well understood, gamma frequency cortical activity has generally been
735 linked to increased spiking activity and network excitation (Yizhar et al., 2011; Cho et al.,
736 2015; Vogt et al,. 2015). In the visual cortex of freely behaving mice, 30-100 Hz broadband
737 gamma activity was found to functionally discriminate between segregated cortical
738 layers of visual processing (Senzai et al., 2019). It was shown that gamma activity can be
739 subdivided into functionally distinct broad- (30-90 Hz) and narrowband (60 Hz) gamma
740 oscillations, which show complementary responses to changes in visual contrast (Saleem

et al., 2017). While narrowband gamma has been associated with thalamocortical communication, broadband gamma power is thought to represent corticocortical communication. Our recordings did not allow to distinguish between underlying network mechanisms, but the broad increase in high gamma band activity we observed in the TFR deviant minus standard difference plots could reflect increased corticocortical network activity during deviance processing. This could suggest involvement of the prefrontal cortex, in line with what was found in human vMMN studies (Yucel et al., 2007; Kimura et al., 2010; Kimura et al., 2011), although no robust visual evoked responses were recorded from our prefrontal cortex electrode. The presence of induced broadband gamma responses thus seems to suggest communication between the visual cortex and other cortical, possibly frontal, areas during visual deviance detection. However, the functional significance of EEG activity in certain frequency bands remains to be assessed, thus hypotheses related to these specific frequency bands should be interpreted carefully.

In conclusion, we developed the first, robust and repeatable vMMN paradigm based on changes in light intensity in freely behaving mice. Our paradigm provides a functional outcome measure for visual processing in these mice. Because no head fixation is needed, our paradigm minimizes animal discomfort while increasing behavioural relevance. The paradigm can easily be implemented to assess sensory processing deficits in mouse models of brain disease, and has the possibility to be compared with experiments in humans which increases translatability of preclinical outcomes.

Acknowledgements

764 This work was supported by a ZonMW TOP [grant number 91216021, 2017, awarded to
765 HB and MJK] and the national Medical NeuroDelta [awarded to AvdM].

766 **Declaration of interest**

767 None

768 **Author contribution statement**

769 **Renate Kat:** Conceptualization, methodology, investigation, formal analysis,
770 visualization, writing – original draft **Berry van der Berg:** Formal analysis, visualization,
771 writing – reviewing & editing **Matthijs JL Perenboom:** Methodology, software **Maarten**
772 **Schenke:** Investigation **Arn MJM van den Maagdenberg:** Resources, funding
773 acquisition, writing – review & editing **Hilgo Bruining:** Funding acquisition, writing –
774 review & editting **Else A Tolner:** Conceptualization, writing – reviewing & editing,
775 supervision **Martien JH Kas:** Conceptualization, funding acquisition, writing – reviewing
776 & editing, supervision

777

778 **References**

779 Ahnaou, A., Moechars, D., Raeymaekers, L., Biermans, R., Manyakov, N. V., Bottelbergs, A.,
780 Wintmolders, C., Van Kolen, K., Van De Casteele, T., Kemp, J.A., Drinkenburg, W.H.,
781 2017. Emergence of early alterations in network oscillations and functional
782 connectivity in a tau seeding mouse model of Alzheimer's disease pathology. Sci.
783 Rep. 7, 1–14. https://doi.org/10.1038/s41598-017-13839-6

784 Baker, M., 2013. Neuroscience: Through the eyes of a mouse. Nature 502, 156–158.
785 https://doi.org/10.1038/502156a

Bates, D., Kliegl, R., Vasishth, S., Baayen, H., 2015a. Parsimonious Mixed Models. ArXiv e-print 1506.04967v2.

Bates, D., Maechler, M., Bolker, B., Walker, S., 2015b. Package lme4. J. Stat. Softw. 67, 1–91. https://doi.org/http://lme4.r-forge.r-project.org

Carrillo-Reid, L., Han, S., Yang, W., Akrouh, A., Yuste, R., 2019. Controlling Visually Guided Behavior by Holographic Recalling of Cortical Ensembles. Cell 178, 447-457.e5. https://doi.org/10.1016/j.cell.2019.05.045

Chen, C.C., Kiebel, S.J., Kilner, J.M., Ward, N.S., Stephan, K.E., Wang, W.J., Friston, K.J., 2012. A dynamic causal model for evoked and induced responses. Neuroimage 59, 340–348. https://doi.org/10.1016/j.neuroimage.2011.07.066

Cho, K.K.A., Hoch, R., Lee, A.T., Patel, T., Rubenstein, J.L.R., Sohal, V.S., 2015. Gamma rhythms link prefrontal interneuron dysfunction with cognitive inflexibility in dlx5/6+/- mice. Neuron 85, 1332–1343. https://doi.org/10.1016/j.neuron.2015.02.019

Clapp, W.C., Eckert, M.J., Teyler, T.J., Abraham, W.C., 2006. Rapid visual stimulation induces N-methyl-D-aspartate receptor-dependent sensory long-term potentiation in the rat cortex. Neuroreport 17, 511–515. https://doi.org/10.1097/01.wnr.0000209004.63352.10

Cohen, M.X., 2014. Analyzing neural time series data: theory and practice, 1st ed. The MIT press, Cambridge, Massachusetts.

Crescitelli, F., Gardner, E., 1961. Correspondences in the behavior of the electroretinogram and of the potentials evoked at the visual cortex. J. Gen. Physiol. 44, 911–928. https://doi.org/10.1085/jgp.44.5.911

Czigler, I., 2007. Visual mismatch negativity: Violation of nonattended environmental regularities. J. Psychophysiol. 21, 224–230. https://doi.org/10.1027/0269-8803.21.34.224

Czigler, I., Weisz, J., Winkler, I., 2006. ERPs and deviance detection: Visual mismatch negativity to repeated visual stimuli. Neurosci. Lett. 401, 178–182. https://doi.org/10.1016/j.neulet.2006.03.018

File, D., File, B., Bodnár, F., Sulykos, I., Kecskés-Kovács, K., Czigler, I., 2017. Visual mismatch negativity (vMMN) for low- and high-level deviances: A control study. Attention, Perception, Psychophys. 79, 2153–2170. https://doi.org/10.3758/s13414-017-1373-y

Fournier, J., Saleem, A.B., Diamanti, E.M., Wells, M.J., Harris, K.D., Carandini, M., 2020. Mouse Visual Cortex Is Modulated by Distance Traveled and by Theta Oscillations. Curr. Biol. 30, 3811-3817.e6. https://doi.org/10.1016/j.cub.2020.07.006

Garrido, M.I., Kilner, J.M., Stephan, K.E., Friston, K.J., 2009. The mismatch negativity: A review of underlying mechanisms. Clin. Neurophysiol. 120, 453–463. https://doi.org/10.1016/j.clinph.2008.11.029

Gelman, a, Hill, J., 2007. Data analysis using regression and multilevel/hierarchical models. Policy Anal. 1–651. https://doi.org/10.2277/0521867061

Grimm, S., Escera, C., Nelken, I., 2016. Early indices of deviance detection in humans and animal models. Biol. Psychol. 116, 23–27. https://doi.org/10.1016/j.biopsycho.2015.11.017

Hamm, J.P., Shymkiv, Y., Mukai, J., Gogos, J.A., Yuste, R., 2020. Aberrant Cortical Ensembles and Schizophrenia-like Sensory Phenotypes in Setd1a+/− Mice. Biol.

832 Psychiatry 88, 215–223. https://doi.org/10.1016/j.biopsych.2020.01.004

833 Hamm, J.P., Yuste, R., 2016. Somatostatin Interneurons Control a Key Component of
834 Mismatch Negativity in Mouse Visual Cortex. Cell Rep. 16, 597–604.
835 https://doi.org/10.1016/j.celrep.2016.06.037

836 Hansen, I.H., Agerskov, C., Arvastson, L., Bastlund, J.F., Sørensen, H.B.D., Herrik, K.F.,
837 2019. Pharmaco-electroencephalographic responses in the rat differ between
838 active and inactive locomotor states. Eur. J. Neurosci. 50, 1948–1971.
839 https://doi.org/10.1111/ejn.14373

840 Harms, L., Michie, P.T., Näätänen, R., 2016. Criteria for determining whether mismatch
841 responses exist in animal models: Focus on rodents. Biol. Psychol. 116, 28–35.
842 https://doi.org/10.1016/j.biopsycho.2015.07.006

843 Heintz, T., Hinojosa, A., Lagnado, L., 2020. Opposing forms of adaptation in mouse visual
844 cortex are controlled by distinct inhibitory microcircuits and gated by locomotion.
845 BioRxiv. https://doi.org/10.1101/2020.01.16.909788

846 Hesse, P.N., Schmitt, C., Klingenhoefer, S., Bremmer, F., 2017. Preattentive processing of
847 numerical visual information. Front. Hum. Neurosci. 11, 1–14.
848 https://doi.org/10.3389/fnhum.2017.00070

849 Hubel, D., Wiesel, T., 1968. Receptive Fields and Functional Architecture of Monkey
850 Striate Cortex. J. Physiol. 195, 215–243.
851 https://doi.org/10.1113/jphysiol.1968.sp008455

852 Hubel, D.H., 1959. Single unit activity in striate cortex of unrestrained cats. J. Physiol.
853 147, 226–238. https://doi.org/10.1113/jphysiol.1959.sp006238

854 Jones, S.R., 2016. When brain rhythms aren't 'rhythmic': implication for their

855 mechanisms and meaning. Curr. Opin. Neurobiol. 40, 72–80.
856 https://doi.org/10.1016/j.conb.2016.06.010

857 Keller, A.J., Martin, K.A.C., 2015. Local circuits for contrast normalization and adaptation
858 investigated with two-photon imaging in cat primary visual cortex. J. Neurosci. 35,
859 10078–10087. https://doi.org/10.1523/JNEUROSCI.0906-15.2015

860 Kimura, M., 2012. Visual mismatch negativity and unintentional temporal-context-based
861 prediction in vision. Int. J. Psychophysiol. 83, 144–155.
862 https://doi.org/10.1016/j.ijpsycho.2011.11.010

863 Kimura, M., Kondo, H., Ohira, H., Schröger, E., 2011. Unintentional temporal context-
864 based prediction of emotional faces: An electrophysiological study. Cereb. Cortex
865 22, 1774–1785. https://doi.org/10.1093/cercor/bhr244

866 Kimura, M., Ohira, H., Schröger, E., 2010a. Localizing sensory and cognitive systems for
867 pre-attentive visual deviance detection: An sLORETA analysis of the data of Kimura
868 et al. (2009). Neurosci. Lett. 485, 198–203.
869 https://doi.org/10.1016/j.neulet.2010.09.011

870 Kimura, M., Widmann, A., Schröger, E., 2010b. Human visual system automatically
871 represents large-scale sequential regularities. Brain Res. 1317, 165–179.
872 https://doi.org/10.1016/j.brainres.2009.12.076

873 Kojouharova, P., File, D., Sulykos, I., Czigler, I., 2019. Visual mismatch negativity and
874 stimulus-specific adaptation: the role of stimulus complexity. Exp. Brain Res. 237,
875 1179–1194. https://doi.org/10.1007/s00221-019-05494-2

876 Kuznetsova, A., Brockhoff, P.B., Christensen, R.H.B., 2017. lmerTest Package: Tests in
877 Linear Mixed Effects Models. J. Stat. Softw. 82, 1–26.

https://doi.org/10.18637/jss.v082.i13

Lopez, L., Brusa, A., Fadda, A., Loizzo, S., Martinangeli, A., Sannita, W.G., Loizzo, A., 2002. Modulation of flash stimulation intensity and frequency: Effects on visual evoked potentials and oscillatory potentials recorded in awake, freely moving mice. Behav. Brain Res. 131, 105–114. https://doi.org/10.1016/S0166-4328(01)00351-5

Luke, S.G., 2017. Evaluating significance in linear mixed-effects models in R. Behav. Res. Methods 1494–1502. https://doi.org/10.3758/s13428-016-0809-y

Maris, E., Oostenveld, R., 2007. Nonparametric statistical testing of EEG- and MEG-data. J. Neurosci. Methods 164, 177–190. https://doi.org/10.1016/j.jneumeth.2007.03.024

Matuoka, T., Yabe, H., Shinozaki, N., Sato, Y., Hiruma, T., Ren, A., Hara, E., Kaneko, S., 2006. The Development of Memory Trace Depending on the Number of the Standard Stimuli. Clin. EEG Neurosci. 37, 223–229. https://doi.org/10.1177/155005940603700312

Matuschek, H., Kliegl, R., Vasishth, S., Baayen, H., Bates, D., 2017. Balancing Type I error and power in linear mixed models. J. Mem. Lang. 94, 305–315. https://doi.org/10.1016/j.jml.2017.01.001

May, P., Tiitinen, H., Ilmoniemi, R.J., Nyman, G., Taylor, J.G., Näätänen, R., 1999. Frequency change detection in human auditory cortex. J. Comput. Neurosci. 6, 99–120. https://doi.org/10.1023/A:1008896417606

Montijn, J.S., Olcese, U., Pennartz, C.M.A., 2016. Visual stimulus detection correlates with the consistency of temporal sequences within stereotyped events of V1 neuronal population activity. J. Neurosci. 36, 8624–8640.

https://doi.org/10.1523/JNEUROSCI.0853-16.2016

Näätänen, R., Sussman, E.S., Salisbury, D., Shafer, V.L., 2014. Mismatch negativity (MMN) as an index of cognitive dysfunction. Brain Topogr. 27, 451–466. https://doi.org/10.1007/s10548-014-0374-6

Oostenveld, R., Fries, P., Maris, E., Schoffelen, J.M., 2011. FieldTrip: Open source software for advanced analysis of MEG, EEG, and invasive electrophysiological data. Comput. Intell. Neurosci. 2011. https://doi.org/10.1155/2011/156869

Park, J., van den Berg, B., Chiang, C., Woldorff, M.G., Brannon, E.M., 2018. Developmental trajectory of neural specialization for letter and number visual processing. Dev. Sci. 21, 1–14. https://doi.org/10.1111/desc.12578

Pazo-Alvarez, P., Cadaveira, F., Amenedo, E., 2003. MMN in the visual modality: A review. Biol. Psychol. 63, 199–236. https://doi.org/10.1016/S0301-0511(03)00049-8

Perenboom, T., Schenke, M., Ferrari, M., Terwindt, G., van den Maagdenberg, A., Tolner, E., 2020. Responsivity to light in familial hemiplegic migraine type 1 mutant mice reveals frequency-dependent enhancement of visual network excitability. Eur. J. Neurosci. 53, 1672–1686. https://doi.org/10.1111/ejn.15041

Sabri, M., Campbell, K.B., 2001. Effects of sequential and temporal probability of deviant occurrence on mismatch negativity. Cogn. Brain Res. 12, 171–180. https://doi.org/10.1016/S0926-6410(01)00026-X

Saleem, A.B., Lien, A.D., Krumin, M., Haider, B., Rosón, M.R., Ayaz, A., Reinhold, K., Busse, L., Carandini, M., Harris, K.D., Carandini, M., 2017. Subcortical Source and Modulation of the Narrowband Gamma Oscillation in Mouse Visual Cortex. Neuron

93, 315–322. https://doi.org/10.1016/j.neuron.2016.12.028

Sanchez-Vives, M. V., Nowak, L.G., McCormick, D.A., 2000. Cellular mechanisms of long-lasting adaptation in visual cortical neurons in vitro. J. Neurosci. 20, 4286–4299. https://doi.org/10.1523/jneurosci.20-11-04286.2000

Sassenhagen, J., Draschkow, D., 2019. Cluster-based permutation tests of MEG/EEG data do not establish significance of effect latency or location. Psychophysiology 56, 1–8. https://doi.org/10.1111/psyp.13335

Sato, Y., Yabe, H., Hiruma, T., Sutoh, T., Shinozaki, N., Nashida, T., Kaneko, S., 2000. The effect of deviant stimulus probability on the human mismatch process. Neuroreport 11, 3703–3708. https://doi.org/10.1097/00001756-200011270-00023

Sculthorpe, L.D., Ouellet, D.R., Campbell, K.B., 2009. MMN elicitation during natural sleep to violations of an auditory pattern. Brain Res. 1290, 52–62. https://doi.org/10.1016/j.brainres.2009.06.013

Senzai, Y., Fernandez-Ruiz, A., Buzsáki, G., 2019. Layer-Specific Physiological Features and Interlaminar Interactions in the Primary Visual Cortex of the Mouse. Neuron 101, 500-513.e5. https://doi.org/10.1016/j.neuron.2018.12.009

Sohya, K., Kameyama, K., Yanagawa, Y., Obata, K., Tsumoto, T., 2007. GABAergic neurons are less selective to stimulus orientation than excitatory neurons in layer II/III of visual cortex, as revealed by in vivo functional Ca2+ imaging in transgenic mice. J. Neurosci. 27, 2145–2149. https://doi.org/10.1523/JNEUROSCI.4641-06.2007

Solomon, S.G., Kohn, A., 2014. Moving Sensory Adaptation beyond Suppressive Effects in Single Neurons. Curr. Biol. 24, R1012–R1022. https://doi.org/10.1016/j.cub.2014.09.001.Moving

947 Stagg, C., Hindley, P., Tales, A., Butler, S., 2004. Visual mismatch negativity: the detection
948 of stimulus change. Neuroreport 15, 487–491.
949 https://doi.org/10.1097/01.wnr.00001

950 Stothart, G., Kazanina, N., 2013. Oscillatory characteristics of the visual mismatch
951 negativity; what evoked potentials aren't telling us. Front. Hum. Neurosci. 7, 1–9.
952 https://doi.org/10.3389/fnhum.2013.00426

953 Sulykos, I., Czigler, I., 2014. Visual mismatch negativity is sensitive to illusory brightness
954 changes. Brain Res. 1561, 48–59. https://doi.org/10.1016/j.brainres.2014.03.008

955 Suzuki, T.H., Nunokawa, S., Jacobson, J.H., 1972. Visually evoked cortical response in
956 light-adapted cat and liminal brightness discrimination. Jpn. J. Physiol. 22, 157–175.

957 Tada, M., Kirihara, K., Mizutani, S., Uka, T., Kunii, N., Koshiyama, D., Fujioka, M., Usui, K.,
958 Nagai, T., Araki, T., Kasai, K., 2019. Mismatch negativity (MMN) as a tool for
959 translational investigations into early psychosis: A review. Int. J. Psychophysiol.
960 145, 5–14. https://doi.org/10.1016/j.ijpsycho.2019.02.009

961 Van Diepen, H.C., Ramkisoensing, A., Peirson, S.N., Foster, R.G., Meijer, J.H., 2013.
962 Irradiance encoding in the suprachiasmatic nuclei by rod and cone photoreceptors.
963 FASEB J. 27, 4204–4212. https://doi.org/10.1096/fj.13-233098

964 Vinken, K., Vogels, R., Op de Beeck, H., 2017. Recent Visual Experience Shapes Visual
965 Processing in Rats through Stimulus-Specific Adaptation and Response
966 Enhancement. Curr. Biol. 27, 914–919. https://doi.org/10.1016/j.cub.2017.02.024

967 Vogt, D., Cho, K.K.A., Lee, A.T., Sohal, V.S., Rubenstein, J.L.R., 2015. The
968 Parvalbumin/Somatostatin Ratio Is Increased in Pten Mutant Mice and by Human
969 PTEN ASD Alleles. Cell Rep. 11, 944–956.

https://doi.org/10.1016/j.celrep.2015.04.019

Warden, M.R., Cardin, J.A., Deisseroth, K., 2014. Optical neural interfaces. Annu. Rev. Biomed. Eng. 16, 103–129. https://doi.org/10.1146/annurev-bioeng-071813-104733

Yan, T., Feng, Y., Liu, T., Wang, L., Mu, N., Dong, X., Liu, Z., Qin, T., Tang, X., Zhao, L., 2017. Theta oscillations related to orientation recognition in unattended condition: A vMMN study. Front. Behav. Neurosci. 11, 1–8. https://doi.org/10.3389/fnbeh.2017.00166

Yizhar, O., Fenno, L.E., Prigge, M., Schneider, F., Davidson, T.J., Shea, D.J.O., Sohal, V.S., Goshen, I., Finkelstein, J., Paz, J.T., Stehfest, K., Fudim, R., Ramakrishnan, C., Huguenard, J.R., Hegemann, P., Deisseroth, K., 2011. Neocortical excitation / inhibition balance in information processing and social dysfunction. Nature 477, 171–178. https://doi.org/10.1038/nature10360

Yucel, G., McCarthy, G., Belger, A., 2007. fMRI reveals that involuntary visual deviance processing is resource limited. Neuroimage 34, 1245–1252. https://doi.org/10.1016/j.neuroimage.2006.08.050

Zhang, D., Yu, B., Liu, J., Jiang, W., Xie, T., Zhang, R., Tong, D., Qiu, Z., Yao, H., 2017. Altered visual cortical processing in a mouse model of MECP2 duplication syndrome. Sci. Rep. 7, 1–14. https://doi.org/10.1038/s41598-017-06916-3

991 **Supplementary Material**

992

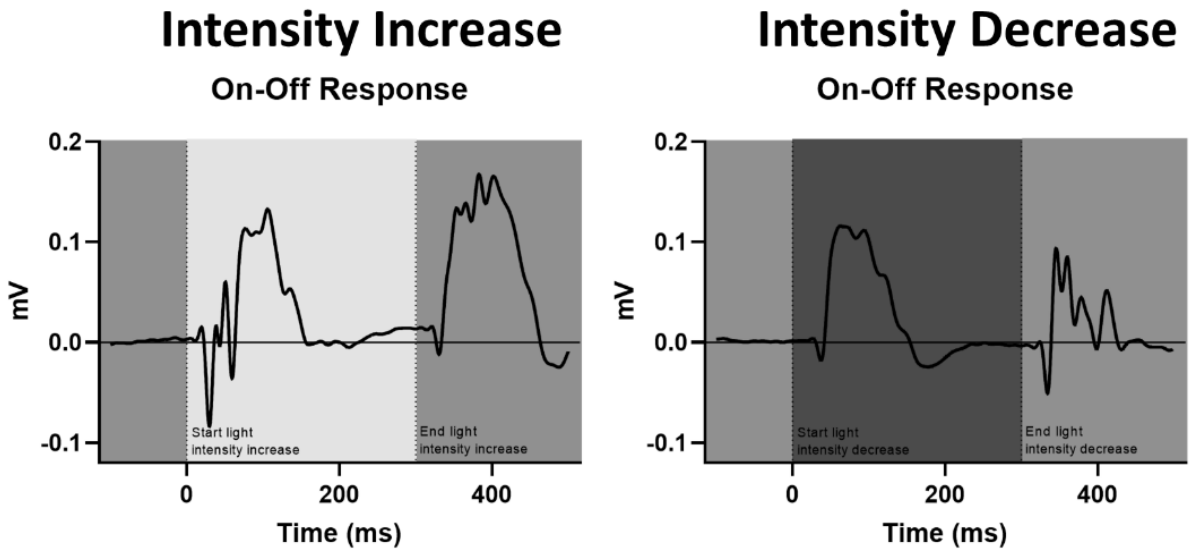

993

994 *Figure S1.* **Comparison of VEP waveforms for the On- and Off-responses to a light**
995 **intensity increase versus light intensity decrease.** Light stimuli lasted for 300 ms,
996 whereby these plots show the 'On-response' to the start of the 300-ms intensity increase
997 or decrease as well as the VEP 'Off-response' to the light intensity changing back to
998 baseline level. The On-response of the light increase, as well as the Off-response of the
999 light decrease, concern a response to an increase in light intensity. The On-response of
1000 the light decrease, as well as the Off-response of the light increase, concern a response to
1001 a light intensity decrease. Presented data show the responses to a light increase and
1002 decrease, averaged over all mice for right and left V1 responses and 2 recordings on
1003 separate days.